

New Insight on the Unusually High Ionic Mobility in Chevrel Phases

E. Levi,^{*,†} G. Gershinsky,[†] D. Aurbach,[†] O. Isnard,^{‡,§} and G. Ceder^{||}

Department of Chemistry, Bar-Ilan University, Ramat-Gan, Israel 52900, Institut Néel, CNRS, associé à l'Université de Grenoble J. Fourier, BP166X, 38042 Grenoble cédex 9, France, Institut Laue Langevin, BP 156 X, 38042 Grenoble cédex 9, France, and Department of Materials Science and Engineering, Massachusetts Institute of Technology, Cambridge, Massachusetts 02139

Received January 6, 2009. Revised Manuscript Received February 16, 2009

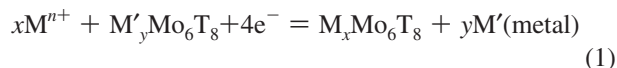
Chevrel Phases (CPs), M_xT_8 ($M = \text{metal}$, $T = \text{S, Se}$) are unique materials, which allow for a fast and reversible insertion of various cations at RT. Earlier, CPs were divided into two major types: type I with large immobile cations, which block any ionic transport in the diffusion channels, and type II with small mobile cations. Our analysis of available experimental data shows that the transport behavior in CPs cannot be understood in the framework of the blocking concept; it is much more complex and includes: (i) apparent immobility of the large M cations like Pb^{2+} , Sn^{2+} , Ag^+ in the ternary phases, MMo_6T_8 ; (ii) coupled $M + M'$ diffusion in the quaternary phases, $M_xM'_y\text{Mo}_6\text{T}_8$, where both large and small cations can assist; (iii) cation trapping in the $\text{Mg}-\text{Mo}_6\text{S}_8$, $\text{Cd}-\text{Mo}_6\text{S}_8$, and $\text{Na}-\text{Mo}_6\text{T}_8$ systems; (iv) a combination of low and high rate diffusion kinetics at the first and last intercalation stages, respectively, for the $\text{Cu}-\text{Mo}_6\text{S}_8$, $\text{Mn}-\text{Mo}_6\text{S}_8$, and $\text{Cd}-\text{Mo}_6\text{Se}_8$ systems; and (v) a fast ionic transport for small cations like Ni^{2+} , Zn^{2+} , and Li^+ . A general structural approach (analysis of the polyhedral linkage in the diffusion channels of CPs and mapping of all the cation sites combined with their bond valence sum values and the distances from the adjacent Mo atoms) used for the first time for a variety of CPs shows two competing diffusion pathways of inserted ions for most of CPs: circular motion within the same cavity between the Mo_6T_8 blocks with activation energy E_c , and progressive diffusion from one cavity to the adjacent one with activation energy E_d . The character of the ionic transport depends mostly on the distribution of the repulsive forces for the inserted cations, as well as on the E_d/E_c ratio, affected in turn by the cation position, its size, cation–Mo interactions, and the anion nature.

Introduction

There is no question that rechargeable Li (ion) batteries are recently the leader in the market of high-energy-density power sources, but their safety and cost limitations stimulate the search for more systems for energy storage and conversion based on other active metals such as magnesium, aluminum, and zinc. One of the major problems of such systems is slow transport of the respective ions in inorganic hosts that can serve as cathodes for such batteries. Until now, only one family of materials, namely Chevrel phases (CPs), $M_x\text{Mo}_6\text{T}_8$ ($M = \text{metal}$, $T = \text{S, Se}$), is known to allow for a fast and reversible insertion of various cations, monovalent (Li^+ , Na^+ , Cu^+) as well as divalent: Zn^{2+} , Cd^{2+} , Ni^{2+} , Mn^{2+} , Co^{2+} , Fe^{2+} , and Mg^{2+} at ambient temperatures,^{1–15} which is

associated with high electronic conductivity of the intercalation compounds.

Amazingly, these compounds can undergo reversible insertion–displacement reactions as well, in which the insertion of one type of cations, $M^{n+} = \text{Li}^+$, Na^+ , Mg^{2+} , or Zn^{2+} , in CPs may be accompanied by extraction of another cation, $M'^{n'+} = \text{Na}^+$, Cu^+ , Ag^+ , Ni^{2+} , In^+ , Fe^{2+} , or Co^{2+} (which exists in the pristine material) and its reduction, leading to the formation of metallic clusters as the reaction product^{3,4,16,17}



Here the reaction suggests a coupled $M-M'$ cations' motion in the crystal structure of the quaternary compounds,

* Corresponding author. E-mail: elenal@mail.biu.ac.il.

[†] Bar-Ilan University.

[‡] Institut Néel.

[§] Institut Laue Langevin.

^{||} Massachusetts Institute of Technology.

- (1) Schollhorn, R.; Kumpers, M.; Besenhard, J. O. *Mater. Res. Bull.* **1977**, *12*, 781.
- (2) Schollhorn, R. *Angew. Chem., Int. Ed.* **1980**, *19*, 983.
- (3) Schollhorn, R. In *Inclusion Compounds*, version 1; Atwood, J. L., Ed.; Academic Press: London, 1984.
- (4) Tarascon, J. M.; Hull, G. W.; Marsh, P.; Ter Haar, L. W. *J. Solid State Chem.* **1987**, *66*, 204.
- (5) Gocke, E.; Schramm, W.; Dolscheid, P.; Schollhorn, R. *J. Solid State Chem.* **1987**, *70*, 71.
- (6) Gocke, E.; Schollhorn, R.; Aselmann, G.; Muller-Warmuth, W. *Inorg. Chem.* **1987**, *26*, 1805.
- (7) Weppner, W.; Huggins, R. A. *Annu. Rev. Mater. Sci.* **1978**, *8*, 269.

(8) Boulanger, C.; Lecuire, J.-M. *Electrochem. Acta* **1987**, *32*, 345.

(9) Boulanger, C.; Lecuire, J.-M. *Electrochem. Acta* **1988**, *33*, 1561. 1567; 1573.

(10) Janssen, M.; Eckert, H.; Muller-Warmuth, W.; Stege, U.; Schollhorn, R. *Chem. Mater.* **1998**, *10*, 3459.

(11) Ritter, C.; Gocke, E.; Fischer, C.; Schollhorn, R. *J. Mater. Res. Bull.* **1992**, *27*, 1217.

(12) Ritter, C.; Noldeke, C.; Press, W.; Stege, U.; Schollhorn, R. *Zeitschrift für Physik B* **1993**, *92*, 437.

(13) Fischer, C.; Gocke, E.; Stege, U.; Schollhorn, R. *J. Solid State Chem.* **1993**, *102*, 54.

(14) Aurbach, D.; Lu, Z.; Schechter, A.; Gofer, Y.; Gizbar, H.; Turgeman, R.; Cohen, Y.; Moskovich, M.; Levi, E. *Nature* **2000**, *407*, 724.

(15) Seghir, S.; Boulanger, C.; Diliberto, S.; Lecuire, J.-M.; Potel, M.; Merdrignac-Conanec, O. *Electrochem. Commun.* **2008**, *10*, 1505.

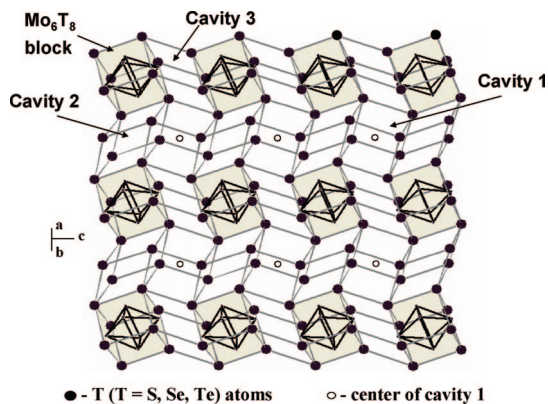


Figure 1. Basic CPs' crystal structure: three types of cavities between Mo_6T_8 blocks. The face-sharing pseudocubes of cavities 1 and 2 form the channels in direction c (one of three equivalent directions in rhombohedral crystals).

$\text{M}_x\text{M}'_y\text{Mo}_6\text{T}_8$.^{16,17} These unusual effects were discovered for the first time about 30 years ago, but most of the subsequent work was devoted to other attractive properties of CPs: electric, thermoelectric, magnetic, and catalytic. Recent application of Mo_6T_8 as unique cathodes for rechargeable Mg batteries^{14,18,19} increased our interest in studying cation mobility in CPs. For further development of new electrode materials for rechargeable Mg batteries, it seems very important first to understand in detail the interesting transport phenomena related to CPs. It is necessary to revise our knowledge about the diffusion processes in these unique compounds.

In spite of variation in symmetry (triclinic or rhombohedral), the crystal structure of all CPs is basically the same: a stacking of Mo_6T_8 blocks (or Mo_6 -octahedral clusters inside anion cubes) with a system of open three-dimensional channels formed by face-sharing pseudocubic cavities 1 and 2 available for cation insertion (a strong repulsion between the Mo atoms and inserting cations does not allow the occupation of cavity 3) (Figure 1).^{20–25} In earlier studies,^{3,5} the unusually high mobility of small divalent cations in CPs was explained by quasi-monovalent state of these cations as transients, which results from a rapid one-electron transfer via the Mo_6T_8 matrix, e.g., $\text{Zn}^{2+} + e^- \leftrightarrow \text{Zn}^+$. In addition, it was assumed^{20,21} that the rhombohedral symmetry of CPs with small cations (radius $< 1 \text{ \AA}$) is associated with a cation motion between equivalent sites, whereas the atomic “free-

ing” in one of the sites at a certain critical temperature is responsible for the triclinic distortion. Previously,²⁶ we presented alternative explanation for a high mobility of multivalent cations in CPs, which was ascribed to a fast and efficient attainment of local electroneutrality by the octahedral Mo_6 clusters. It was also shown²⁴ that there is no direct correlation between the CPs symmetry and the cation mobility. This paper is devoted to the effect of the cation nature on its diffusivity in CPs.

In general, cation transport in all CPs proceeds via vacant sites in cavities 1 and 2, but the environment and the arrangement of these sites inside the cavities differ surprisingly for different compositions.^{20–25} According to the cation position in the crystal structure and its ionic mobility, all the $\text{M}_x\text{Mo}_6\text{T}_8$ compounds were divided earlier^{3,20,21} into two major groups: type I with constant $x = 1$ and large (radius $> 1 \text{ \AA}$) immobile cations located exactly in (or very close to) the origin of cavity 1 (Figure 1), and type II with highly mobile, small (radius $< 1 \text{ \AA}$) ions shifted (“delocalized”) from the origin, where x is limited by four electrons per Mo_6 cluster. In the latter case, the arrangement of the cation sites was described as inner (six equivalent tetrahedral sites in cavity 1) and outer (six equivalent tetrahedral sites located in six adjacent cavities 2) rings. It was also shown^{20,21} that the value of the cation delocalization depends mostly on the cation size: the smaller the cation, the higher is its shift from the origin of cavity 1. Thus, it was commonly accepted that the main parameter, which affects the cation mobility in CPs, is its size. However, the reason of the completely different mobility of large and small cations in CPs was not discussed in detail. It was only mentioned that large cations fall into a combined energetic/steric trap and block any ionic transport.^{3–5} In fact, cavity 1, located on the intersection of the diffusion channels, provides only one site for large cations (in its origin or very close to the origin); thereby, its occupation by immobile ion should stop any ionic motion.

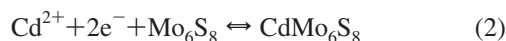
This suggestion agrees well with most of the synthetic results, which showed that CPs of group I could be obtained only at high temperatures, in contrast to CPs of group II, which can be produced by chemical or electrochemical reversible reactions as well at ambient temperatures. However, our analysis of available experimental data^{1,3–11,13,20–22,28–37}

- (16) Levi, E.; Mitelman, A.; Aurbach, D.; Brunelli, M. *Chem. Mater.* **2007**, *19*, 5131, and references therein.
 (17) Mitelman, A.; Levi, M. D.; Lancry, E.; Levi, E.; Aurbach, D. *Chem. Comm.* **2007**, 4212.
 (18) Aurbach, D.; Weissman, I.; Gofer, Y.; Levi, E. *Chem. Rec.* **2003**, *3*, 61.
 (19) Aurbach, D.; Suresh, G. S.; Levi, E.; Mitelman, A.; Mizrahi, O.; Chusid, O.; Brunelli, M. *Adv. Mater.* **2007**, *19*, 4260.
 (20) Yvon, K. In *Current Topics in Material Science*; Kaldis, E. Ed.; North-Holland: Amsterdam, 1979; Vol. 3.
 (21) *Topics in Current Physics: Superconductivity in Ternary Compounds* /Fisher, Ø.; Maple, M. B., Eds.; Springer-Verlag: Berlin, 1982.
 (22) Roche, C.; Chevrel, R.; Jenny, A.; Pecheur, P.; Scherrer, H.; Scherrer, S. *Phys. Rev. B* **1999**, *60*, 16442.
 (23) Belin, S.; Chevrel, R.; Sergent, M. J. *Solid-State Chem.* **2000**, *155*, 250.
 (24) Levi, E.; Mitelman, A.; Aurbach, D.; Isnard, O. *Inorg. Chem.* **2007**, *46*, 7528.
 (25) Levi, E.; Mitelman, A.; Isnard, O.; Brunelli, M.; Aurbach, D. *Inorg. Chem.* **2008**, *47*, 1975.

- (26) Levi, E.; Levi, M. D.; Chasid, O.; Aurbach, D. *J. Electroceram.* **2007**, DOI 10.1007/s10832-007-9370-5.
 (27) Kaidi, Z.; Boulanger, C.; Lecuire, J. M.; Lemee, N.; Guilloux-Viry, M.; Perrin, A. *Solid State Science* **1999**, *1*, 623.
 (28) Tarascon, J. M.; Disalvo, F. J.; Murphy, D. W.; Hull, G. W.; Rietman, E. A.; Waszczak, J. V. *J. Solid State Chem.* **1984**, *54*, 204.
 (29) Tarascon, J. M.; Di Salvo, F. J.; Waszczak, J. V.; Hull, G. W. *Phys. Rev. B* **1985**, *31*, 1012.
 (30) Prigge, C.; Muller-Warmuth, W.; Gocke, E.; Schollhorn, R. *Solid State Ionics* **1993**, *62*, 143.
 (31) Prigge, C.; Muller-Warmuth, W.; Gocke, E.; Schollhorn, R. *Chem. Mater.* **1993**, *5*, 1493.
 (32) Dudley, G. J.; Cheung, K. Y.; Steele, B. C. H. *J. Solid State Chem.* **1980**, *32*, 259.
 (33) Levi, M. D.; Lancry, E.; Gizbar, H.; Lu, Z.; Levi, E.; Gofer, Y.; Aurbach, D. *J. Electrochem. Soc.* **2004**, *151*, A1044.
 (34) Lancry, E.; Levi, E.; Gofer, Y.; Levi, M.; Salitra, G.; Aurbach, D. *Chem. Mater.* **2004**, *16*, 2832.
 (35) Levi, E.; Lancry, E.; Mitelman, A.; Aurbach, D.; Ceder, G.; Morgan, D.; Isnard, O. *Chem. Mater.* **2006**, *18*, 5492.
 (36) Levi, M. D.; Lancry, E.; Levi, E.; Gizbar, H.; Gofer, Y.; Aurbach, D. *Solid State Ionics* **2005**, *176*, 1695.

(Tables 1 and 2) demonstrates that the ion-transport behavior in CPs is much more complex; it includes (i) apparent immobility of the large M cations like Pb^{2+} , Sn^{2+} , Ag^+ in the ternary phases, MMo_6T_8 ; (ii) coupled $\text{M} + \text{M}'$ diffusion in the quaternary phases, $\text{M}_x\text{M}'_y\text{Mo}_6\text{T}_8$, where both large and small cations can assist; (iii) cation trapping in the $\text{Mg}-\text{Mo}_6\text{S}_8$, $\text{Cd}-\text{Mo}_6\text{S}_8$, and $\text{Na}-\text{Mo}_6\text{T}_8$ systems; (iv) a combination of low and high rate diffusion kinetics at the first and last intercalation stages, respectively, for the $\text{Cu}-\text{Mo}_6\text{S}_8$, $\text{Mn}-\text{Mo}_6\text{S}_8$, and $\text{Cd}-\text{Mo}_6\text{Se}_8$ systems; and (v) a fast ionic transport for small cations like Ni^{2+} , Zn^{2+} , and Li^+ . Thus, contrary to general expectation, there is no unambiguous correlation between the cation mobility and its size. Moreover, it is not clear how large cations “blocked” in MMo_6T_8 can move in the same crystal structure upon coupled $\text{M} + \text{M}'$ diffusion (more detailed discussion of the data is presented in the Supporting Information).

It should be mentioned that in the earlier publications, the above experimental results were neither systemized nor defined as typical for the CPs groups. For instance, a partial cation trapping was not recognized for the $\text{Cd}-\text{Mo}_6\text{S}_8$ system.^{5,9} Actually, the first stage of Cd insertion was presented⁵ as fully reversible electrochemical reaction at RT



whereas the formation of $\text{Cd}_2\text{Mo}_6\text{S}_8$ was described⁹ as a difficult process, which occurs very slowly. Furthermore, ref 5 states that the maximal intercalation level that can be reached for $\text{Cd}_x\text{Mo}_6\text{S}_8$ by an electrochemical insertion is $x = 1$. However, the evolution of the electrochemical response for the $\text{Cd}_x\text{Mo}_6\text{S}_{8-y}\text{Se}_y$ ($y = 0, 4, 6, \text{ and } 8$) series with characteristic potentials of Cd insertion, which was presented in ref 9, as well as its similarity with the data for the $\text{Mg}-\text{Mo}_6\text{T}_8$ system^{33–37} allow us to suggest the opposite interpretation of these experimental results: The fast reversible reaction discovered^{5,9} for $\text{Cd}_x\text{Mo}_6\text{S}_8$ should be referred to the second insertion stage ($1 < x < 2$). Moreover, reaction 2 is irreversible even at elevated temperature (60 °C) because of the trapping of Cd^{2+} cations in CdMo_6S_8 , whereas substitution of sulfur atoms by selenium results in the fully reversible Cd^{2+} cations insertion (at 60 °C). Thus, we believe that the transport behavior of Cd^{2+} cations in CPs agrees well with the scheme presented above (see more detailed discussion in the Supporting Information).

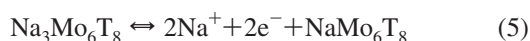
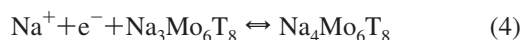
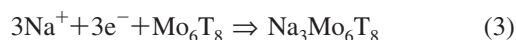
Another important example is the problematic interpretation of the trapping phenomena in the $\text{Na}-\text{Mo}_6\text{T}_8$ systems,^{4,5} which allow for the insertion of four sodium cations per formula unit but subsequent extraction of only three of them. According to the authors,^{4,5} the insertion/deinsertion process is asymmetric: The first phase, which forms upon the electrode reduction, is $\text{Na}_3\text{Mo}_6\text{T}_8$, with high ionic mobility (type II of CPs), whereas NaMo_6T_8 (type I of CPs) can be obtained only upon the cation extraction:

Table 1. Data Related to Mobility of Large Cations in CPs at RT

cation	cation radius for CN = 6 (Å)	host	crystal data for MMo_6T_8	data related to the cation mobility at RT		
				insertion in common powder electrodes	insertion in thin films	coupled diffusion (formation of quaternary compounds and metal extrusion)
K^+	1.33	Mo_6S_8	unknown	e.l.-chem. insertion, maximal $x = 3^1$	insertion in thin films	
Pb^{2+}	1.26	Mo_6S_8	$R\bar{3}$, classic type $I^{20,21}$	not found	chem. insertion, maximal $x = 1^{27}$	e.l.-chem. insertion/deinsertion, maximal $x = 0.2^{27}$
Sn^{2+}	1.02	Mo_6S_8	$R\bar{3}$, classic type $I^{20,21}$	not found	chem. insertion, maximal $x = 1^{27}$	
Ag^+	1.13	Mo_6S_8 , Mo_6Se_8	$R\bar{3}$, classic type $I^{20,21}$	not found	chem. insertion, maximal $x = 1^3$	$(\text{Ag}^+ + \text{Li}^+, \text{Na}^+, \text{Cu}^+, \text{ or } \text{Zn}^{2+})^{3,4,28}$ $(\text{Ag}^+ + \text{Li}^+, \text{Na}^+, \text{Cu}^+, \text{Cd}^{2+}, \text{ or } \text{Zn}^{2+})^3$
In^+	1.30	Mo_6S_8	$R\bar{3}$, type I, CN = 5 ²¹	not found		$(\text{In}^+ \text{ and } \text{In}^{3+} + \text{Li}^+)^{28}$
In^{3+}	0.92	Mo_6S_8	$R\bar{3}$, type I, CN = 5 ²¹	not found		$(\text{Ti}^+ \text{ and } \text{Ti}^{3+} + \text{Li}^+)^{28}$
Ti^+	1.36	Mo_6S_8	$R\bar{3}$, ²⁹ unknown	not found		
Ti^{3+}	1.05	Mo_6S_8	$R\bar{3}$, ²⁹ unknown	not found		

(37) Levi, E.; Lancy, E.; Mitelman, A.; Aurbach, D.; Isnard, O.; Djurado, D. *Chem. Mater.* **2006**, *18*, 3705.

(38) West, A. R. *Basic Solid State Chemistry*; John Wiley & Sons: New York, 1988.



To explain the trapping, the blocking concept for NaMo_6T_8 was used.^{4,5} However, in light of this concept, it is unclear how the immobile Na^+ ions in NaMo_6T_8 allow for further Na insertion and the formation of the intercalation compounds, $\text{Na}_x\text{Mo}_6\text{T}_8$, up to $x = 4$ at RT.

The unusual asymmetric mechanism of Na insertion was confirmed by phase analysis performed by in situ⁴ and ex situ⁵ X-ray diffraction (XRD). However, the researchers^{4,5} presented contradictory conclusions about the symmetry of the $\text{Na}_x\text{Mo}_6\text{S}_8$ ($x = 3$ and 4) phases: They were found to be rhombohedral in the ex situ experiments and triclinic in the in situ one. Thus, it can be suggested that the in situ XRD patterns, obtained upon the first Na insertion for $x = 1$ and assigned by the authors⁴ as a mixture of Mo_6S_8 and triclinic $\text{Na}_3\text{Mo}_6\text{S}_8$, should be related rather to a mixture of three rhombohedral phases, Mo_6S_8 , NaMo_6S_8 , and $\text{Na}_3\text{Mo}_6\text{S}_8$ (a formation of such a mixture is quite possible because of nonequilibrium conditions caused by slow Na diffusion in $\text{Na}_x\text{Mo}_6\text{S}_8$ for $x < 1$). Hence, we believe that Na insertion into Mo_6T_8 follows the same major stages as Li insertion:⁶ $\text{Mo}_6\text{T}_8 \rightarrow \text{MMo}_6\text{T}_8 \rightarrow \text{M}_3\text{Mo}_6\text{T}_8 \rightarrow \text{M}_4\text{Mo}_6\text{T}_8$, $\text{M} = \text{Na}$ or Li , whereas the quite different electrochemical behavior of these systems (obvious Na trapping vs high Li mobility) should be related to the expected structural difference in the cation positions inside cavity 1 for the MMo_6T_8 compounds.

Actually, in our previous work devoted to $\text{Mg}-\text{Mo}_6\text{T}_8$ systems,^{25,26,35,37} we proposed an alternative trapping mechanism: The apparent partial immobility of Mg^{2+} cations upon their extraction from MgMo_6S_8 at RT was explained by the specific features of the CPs crystal structure, namely by the ring arrangement of closely located vacant sites (inner ring) in cavity 1 with low potential energy. At low levels of Mg insertion into Mo_6S_8 , i.e., upon formation of rhombohedral MgMo_6S_8 , such an arrangement should result in a fast circular motion of the Mg^{2+} ions within the same cavity 1, as well as in a high activation barrier for migration between different cavities. Progressive bulk diffusion becomes pos-

sible because of repulsion between inserting cations, i.e., it necessitates the presence of the second cation in the same group of sites (six inner plus six outer sites). As a result, the characteristic features of the system are the overvoltage upon reduction and trapping upon oxidation for $x < 1$, as well as a fast diffusion for $x > 1$ (note that the same features are typical for Na and Cd insertions). In the selenide host, a triclinic distortion caused by Mg insertion changes the geometry of the cation sites and leads to the high Mg mobility in the whole intercalation range ($0 < x < 2$).^{25,26} Trapping can be prevented by using a ternary host, $\text{M}'_y\text{Mo}_6\text{T}_8$. For instance, full reversibility was attained upon Mg insertion into CuMo_6T_8 , as the Cu–Mg repulsion in the cavities results in Mg detrapping.^{16,17}

The aim of the present article is to explain the peculiarities of the cation transport for the CPs variety by using the same structural approach as was applied previously for the separate $\text{Mg}-\text{Mo}_6\text{T}_8$ systems. For this, we analyzed the diffusion routes of different cations in the CPs' crystal structure, especially in the CP compounds formed at the first stages of cation insertion (As was mentioned above, the ionic transport in the compounds with high intercalation level should be normally a priori fast because of cation–cation repulsion). According to the previous efforts in this area,^{24,26} such analysis should be based on the mapping of all the cation sites and requires knowledge of exact crystal structures of the intercalation compounds. Thus, we used the available literature data and performed X-ray and neutron refinements for a number of unknown crystal structures (the experimental results we obtained in this work, devoted to the phase diagrams of several interesting M- Mo_6T_8 systems, will be presented in a separate paper). It should be noted that the CPs related to the present study were chosen according to the availability of information about the ionic mobility of cations in them.

Structural Approach for Understanding Cations Diffusion in CPs

In general, in order to show the relation between structural and transport parameters of any ionic solid and to follow a possible cation pathway upon diffusion, it is necessary (i) to describe the crystal structure as a set of the linked polyhedra (in accordance to the first Pauling's rule), (ii) to

Table 2. Effect of the Cation Character and the Intercalation Level on the Diffusion Kinetics in CPs (case of “small” cations) at RT

cation	cation radius for CN = 6 (Å)	host	exact crystal data for $\text{M}_{-1}\text{Mo}_6\text{T}_8$	diffusion kinetics			ref.
				$x \leq 1$ (or 2 for Cu^+)	$x > 1$ (or 2 for Cu^+)	additional phenomena	
Li^+	0.68	Mo_6Se	$R\bar{3}$, classic type II ¹¹	fast	fast		6, 7, 11, 30, 31
		Mo_6Se_8	$R\bar{3}$, ⁶ unknown	fast	fast		
Ni^{2+}	0.74	Mo_6S_8	$R\bar{3}$, classic type II ^{20,21}	fast	fast		8, 11
		Mo_6Se_8	$R\bar{3}$, new type ²⁰	fast	fast		
Zn^{2+}	0.83	Mo_6T_8	$R\bar{3}$, ⁵ unknown	fast	fast		5
Cu^+	0.98	Mo_6S_8	$R\bar{3}$, classic type II ^{20,21}	slow	fast		13, 32
Mn^{2+}	0.91	Mo_6S_8	$R\bar{3}$, ²¹ unknown	slow	fast		8
		Mo_6Se_8	$P\bar{1}$, new type ²²	fast	fast		
Cd^{2+}	0.99	Mo_6S_8	$R\bar{3}$, ⁵ unknown	slow	fast ^a	trapping for $x < 1$ ^a	5, 9, 10
		Mo_6Se_8	$R\bar{3}$, ⁵ unknown	slow	fast		
Mg^{2+}	0.74	Mo_6S_8	$R\bar{3}$, classic type II ³⁵	slow	fast	trapping for $x < 1$	33–35
		Mo_6Se_8	$P\bar{1}$, classic type II ³⁸	fast	fast		
Na^+	0.98	Mo_6T_8	$R\bar{3}$, ⁵ unknown	slow	fast	trapping for $x \leq 1$	4, 5

^a The interpretation of the experimental data related to Cd^{2+} insertion into Mo_6S_8 differs from that of ref 5, 9, and 10 (see text).

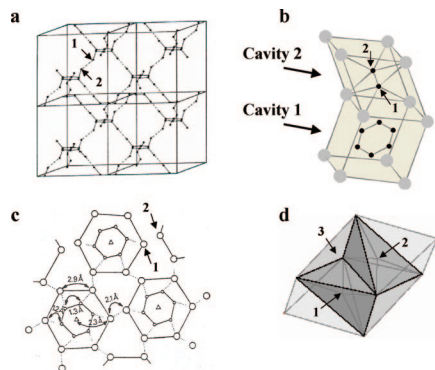


Figure 2. Different descriptions of the cation environments for CPs: (a) Relative arrangement of the inner and outer sites.³⁹ (b) Schematic cation positions inside the cavities.^{23,31} (c) Maps of the cation sites for a few of the CPs.^{11,12,32} (d) Polyhedral structure of cavity 2 for rhombohedral CPs with small cations.^{25,37} Points 1 and 2 mark adjacent outer sites, whereas point 3 denotes one of the central sites in cavity 2.

estimate the activation energy of hopping based on the anion and cation environments around each cation site involved in the diffusion, and (iii) to determine the distances of the cation hopping.³⁸ In the past, such an approach was never fully applied for CPs. Description of the cation environments was restricted to “continuous transition between an eight-fold and a four-fold coordination” of cations in cavity 1,²⁰ relative arrangement of the inner and outer sites (Figure 2a),³⁹ or their schematic positions inside the cavities^{23,31} (Figure 2b). The maps of the cation sites presented for a few CPs^{11,12,32} include nothing more than dimensions of the inner and outer rings and their separation (Figure 2c).

The problem is that the simplified presentations accepted for CPs are insufficiently informative for the diffusion analysis. For instance, a fast diffusion in $\text{Ni}_2\text{Mo}_6\text{S}_8$ was explained¹¹ by short separation between adjacent outer rings, i.e., a direct cation hopping between points 1 and 2 was assumed (Figure 2). However, according to the polyhedral structure of cavity 2 for such compounds,^{25,37} it is clear that the hopping between these sites is not direct, but should include an additional transport step in the neighboring tetrahedral interstitials (point 3 in Figure 2d). As a result, the distances between adjacent outer rings in CPs might be less important for the cation motion than the environment of the transport site (especially, the distance of the point 3 from Mo atom), because of a crucial influence of the latter on the activation energy of hopping. Thus, our first task in the diffusion analysis is to describe the polyhedral linkages in CPs, in order to determine the positions of all the cation sites (including the transport ones) in the centers of these polyhedra, their environment, and interconnections.

Polyhedral Linkages in CPs. The absence of polyhedral presentations for CPs can be explained by the versatility of their structural types.^{20–25} As a result, the polyhedral linkages inside the pseudocubic cavities 1 and 2, i.e., in the diffusion channels, may be quite different^{25,37} (Figures 3 and 4). In addition, it is not so simple to understand the position and the environment of possible transport sites, which remain vacant at all steady intercalation stages. To see the problem,

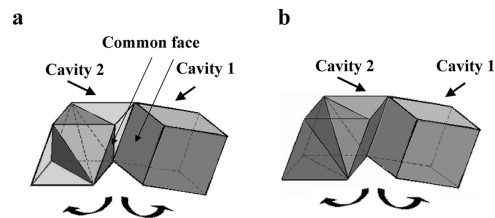


Figure 3. Different choice of the transport sites and polyhedral linkage in cavities 1 and 2 for CPs with large cations: (a) Mismatching between pseudocube of cavity 1 and octahedron in cavity 2 in the case when the transport site is chosen in the origin of cavity 2. (b) Matching between the pseudocube of cavity 1 and the two square pyramids combined with two tetrahedra in cavity 2 (the transport sites are in the centers of these polyhedra). Note that the cavities’ cubes are separated for clarity.

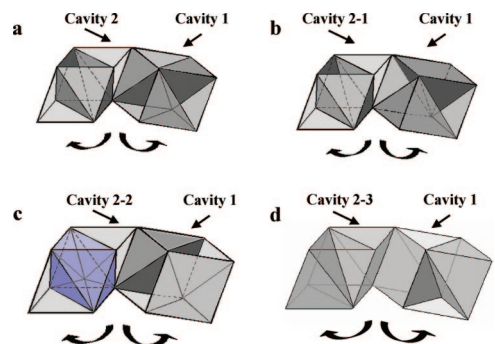


Figure 4. Versatility of the sites’ environments in CPs with small cations: (a) Rhombohedral phases. (b–d) Three different cases of matching between cavities 1 and 2 for triclinic MnMo_6S_8 . The occupied $[\text{MnS}_6]$ octahedron is marked by blue.

let us try to choose the diffusion pathway for hopping of large cations located in the origin of cavity 1 (pseudocubic environment, coordination number (CN) = 8). On the basis of the apparent similarity of the pseudocubic cavities 1 and 2 (Figure 1), it seems logical to suggest that the latter provides only one vacant site in its center with CN = 8. In this case, the sites’ separation, equal to a half-parameter of the rhombohedral unit cell ($\sim 3.3\text{--}3.4$ Å), is really too large for hopping, which would imply that the migration of large multivalent cations is not possible.

However, because of a relatively high and asymmetric compression of cavity 2 in all CPs, the environment of its central site is not cubic, but rather octahedral. Thus, if we choose the transport site in the center of cavity 2, this cavity should be presented as a combination of one octahedron and two tetrahedra (Figure 3a). Looking now at the square face of cavity 2, common for the sharing cubes, one can see that it loses its integrity. This mismatching between polyhedra in cavities 1 and 2 testifies that the hypothesis involving transport site in the center of cavity 2 was wrong. Actually, for CPs of the type I, there is only one way to divide the space of cavity 2 in polyhedra, i.e., the positions of the transport sites in cavity 2 are quite definite: The matching required by the first Pauling’s rule is realized only for a combination of two tetrahedra and two square pyramids in cavity 2 (Figure 3b). Interestingly, such a polyhedral structure agrees well with the data obtained for quaternary compound, $\text{SnFe}_{0.4}\text{Mo}_6\text{S}_8$, where Sn is located in the origin of cavity 1 (CN = 8), whereas Fe occupies the positions close to the usual outer sites, but with a square-pyramidal coordination

(39) Uchida, T.; Tanjo, Y.; Wakihara, M.; Taniuchi, M. *J. Electrochem. Soc.* **1990**, *137*, 7.

(CN = 5).⁴⁰ The distance between the Sn and Fe sites was found to be 2.14 Å, which is quite convenient for cation hopping. Note also that such a polyhedral linkage provides a window of four anions (the pyramids' bases), which is much easier for cation jumping than that of three anions (tetrahedral faces).

Figure 4 illustrates the versatility of the sites' environments in CPs with small cations, which was already discussed in our previous papers.^{25,37} In the CPs hosts, Mo₆T₈, and classic CPs with small cations, such as rhombohedral Cu_xMo₆S₈, both the cavities 1 and 2 are composed of six tetrahedra, but differently linked to each other (Figures 2d and 4a). Another important example is the crystal structure of triclinic MnMo₆S₈, which nicely demonstrates the difference in the polyhedral linkage of three nonequivalent cavities 2 (Crystallographic data for the calculations of the coordination polyhedra can be found in ref 22): (i) six tetrahedra in cavity 2–1 (Figure 4b); (ii) [MnS₆] octahedron linked to two empty tetrahedra in cavity 2–2 (Figure 4c), and iii) a combination of two square-pyramids and two tetrahedra in cavity 2–3 (Figure 4d). Cavity 1 in MnMo₆S₈ has the same polyhedral structure as cavity 2–3 with a wide window of four anions between the cavities (this window may be considered as favorable for cation diffusion). On the basis of the knowledge of these polyhedral linkages, it is possible to go to the second stage of the diffusion analysis: to correlate the structural parameters of the cation sites to the energetic ones.

Mapping of the Cation Sites in CPs. In general, the crystal structure of an intercalation compound can be presented as a map of the equipotential levels, where, at different intercalation stages, the inserted cations occupy subsequently the wells with increasing potential energy. (Note that the potential energy surface will be modified as intercalation proceeds. Thus, it depends not only on the structure of the host but also on the multiple interactions between the ions of the host and the inserting cations) The energy of sites can be predicted by ab initio calculations, but the inconsistent results obtained by two different groups for the Mg–Mo₆S₈ system^{35,41} show that the application of this method for CPs is not simple. Thus, before performing such calculations, it is quite desirable to understand the structural factors that affect the thermodynamics and kinetics of cation insertion.

In previous papers,^{25,37} we used special maps of all the sites (including the transport ones) in cavity 1 and in three adjacent cavities 2 (The latter are equivalent for rhombohedral CP crystals, but different for the triclinic ones.). Typical examples of such maps are presented in Figure 5 (Note that the structure of three additional cavities 2 linked to cavity 1 by common faces is not shown in the maps, but it is identical to that of the presented ones, and it can be obtained by inversion in cavity 1's origin). Here the circles represent the cation sites in the CP's crystal structure, whereas the numbers inside the circles are the bond valence sums (BVS) for these

sites.^{42,43} The closer the BVS to the formal electrostatic charge of the cation in ionic compounds, the more suitable is the size of the anion polyhedron for the cation insertion. The occupied sites are marked by blue color, whereas light and dark gray colors are used to distinguish (according to the BVS values) between empty sites that are suitable and inconvenient for cation intercalation, respectively. Thick circle lines mark the positions that are too close to Mo atoms. All the direct lines connect the centers of the face-sharing polyhedra, i.e., they describe the lengths of possible cation jumps. The only exception is the line between the opposite inner sites, which shows the diameter of the inner ring. The red lines mark possible pathways of the cation motion (See the analysis below). The tables in the maps present the shortest distances between the cation sites M_i and the Mo atoms. Thus, the maps provide information not only about hopping lengths, but also about energetic parameters of the separate jumps (such as potential energies of the cations sites and activation barriers) in the form of the BVS values for the sites and the M_i –Mo distances (additional maps for a variety of CPs with known ionic mobility can be found in the Supporting Information).

Results and Discussion

Two Competing Pathways for Cation Motion in Most of CPs. Figure 5a presents the maps of the cation sites for the host, Mo₆S₈, with the BVS values calculated for Cu⁺ cations (This cation is chosen, because its insertion results in minimal geometric distortion of the initial host structure). According to the BVS and the M_i –Mo distances, the relations between the potential energies of the sites, E_i , should be the following: E_1 of the inner sites < E_2 of the outer sites < E_3 of the central sites of cavity 2 < E_4 of the peripheral sites. The structural data^{20,21} for the sulfides and for a part of the selenides confirm these simple considerations: Cations in these compounds occupy first the interstitials in cavity 1, as the most distant from the Mo atoms, and then the outer sites in cavity 2. This order breaks down only for the CPs' selenides of transition metals,^{22,23} where specific metal–metal interactions between the cations and the Mo atoms result in the occupation of the central sites in cavity 2.

As can be seen in Figure 5a, the crystal structure of the host provides two competing pathways for inserted cations: (i) a circular one between the inner sites, with activation energy E_c and (ii) a progressive diffusion from one cavity 1 (or 2) to the adjacent one, with activation energy E_d . In the latter case, the ionic transport includes four separate jumps: two identical (between inner M_1 and outer M_2 sites) and two different (between outer M_2 and central M_3 sites in cavity 2), with maximal activation energies. The peripheral M_4 sites, as the closest to the Mo atoms in most of CPs, are usually not involved in the diffusion because of strong M–Mo repulsion. These two competing pathways exist also in the majority of the intercalation compounds, M_x Mo₆T₈ (Figure 5b–e; see also the maps in the Supporting Information), whereas the absence of the circular way for cations located

(40) *Ternary Superconductors*; Shenoy, G. K.; Dunlap, B. D.; Fradin, F. Y., Eds.; North-Holland: Amsterdam, 1981.

(41) Kganyago, K. R.; Ngoepe, P. E.; Catlow, C. R. A. *Phys. Rev. B* **2003**, *67*, 104103.

(42) Brese, N. E.; O'Keefe, M. *Acta Crystallogr., Sect. B* **1991**, *47*, 192.

(43) Brown, I. D. *Acta Crystallogr., Sect. B* **1992**, *48*, 553.

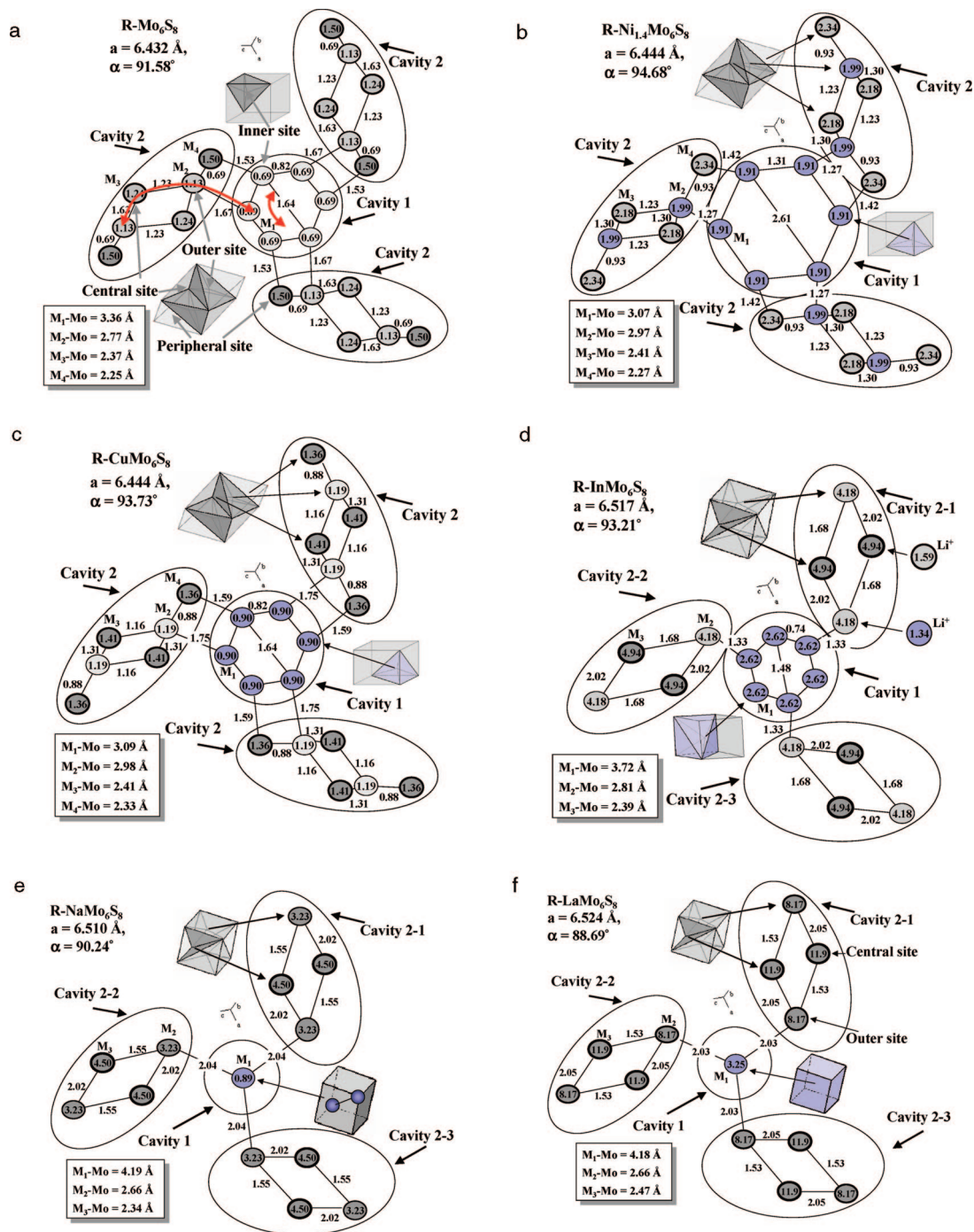


Figure 5. Typical maps of the cation sites for the rhombohedral (R) CPs: (a) Mo_6S_8 , (b) $\text{Ni}_{1.4}\text{Mo}_6\text{S}_8$, (c) CuMo_6S_8 , (d) InMo_6S_8 , (e) NaMo_6S_8 , (f) LaMo_6S_8 . The projections are normal to -3 symmetric axis. The inserts show the polyhedral structure of cavities 1 and 2 (the orientation of the polyhedra is not related to the translation vectors). The occupied sites are colored by blue.

exactly in the origin of cavity 1 (Figure 5e) can be regarded as the limiting case. Below, we present some general considerations concerning the mobility of different cations in CPs.

Factors Affecting the Cation Diffusivity in CPs. Hopping Distances. Figure 6 presents the distances of the separate jumps between the cation sites, $M_1\text{-}M_2$, $M_2\text{-}M_3$, and $M_3\text{-}M_2$ (see the pathway from one cavity 1 to the adjacent one in Figure 5a), and the total pathway lengths of the progressive diffusion, $M_1\text{-}M_2\text{-}M_3\text{-}M_2\text{-}M_1$, in the CPs with different cations as a function of their sizes (or, more precisely, the lengths of the ideal chemical bonds “cation-

anion”^{42,43}). The tendency is very clear: all the distances are longer for bigger cations. However, even for large cations like Pb, Na, Ag, or La, the maximal length of the separate jumps does not exceed 2.3 \AA (For comparison, the distance between adjacent tetrahedral and octahedral sites in spinel, $\text{Li}_x\text{Mn}_2\text{O}_4$, known as a fast Li conductor, is close to 1.8 \AA). Thus, the increase in the hopping lengths for the large cations cannot be the crucial parameter, which limits their mobility in CPs. Moreover, it can be shown (see the Supporting Information) that the potential energy of the square-pyramidal ($\text{CN} = 5$) sites in cavity 1 for CPs with large cations is relatively close to that of the central site. Thus, it is quite

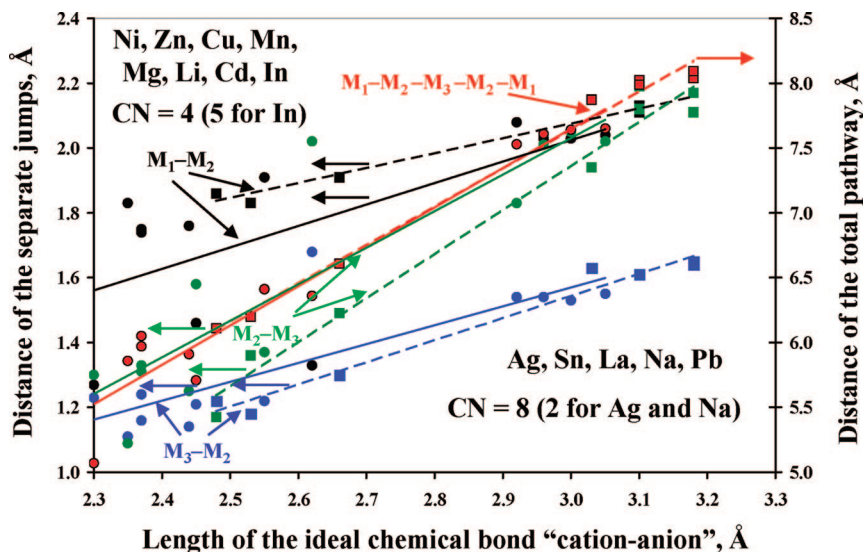


Figure 6. Distances of the separate jumps and the total pathway from one cavity 1 (2) to the adjacent one as a function of the lengths of the ideal chemical bonds “cation–anion”. The solid and dashed lines are related to the sulfides and selenides, respectively.

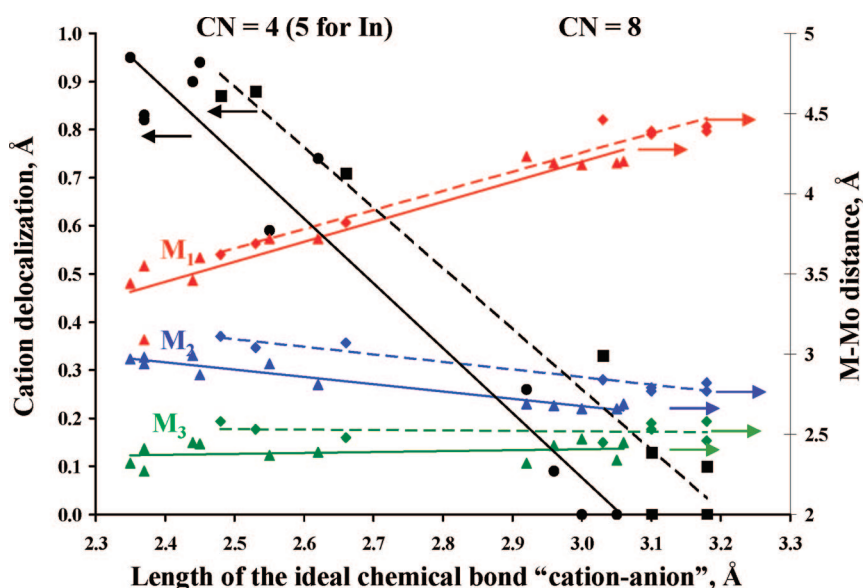


Figure 7. Correlations between the lengths of the ideal chemical bonds “cation–anion”, cations’ delocalization, and the M_i –Mo distances.

possible that formation of such compounds as NaMo_6S_8 proceeds via an intermediate metastable step with shifted cation location and, respectively, lower hopping lengths for separate jumps.

Energetic Characteristics of the Cation Sites and E_d/E_c Ratio. The most obvious characteristic feature of the maps for the $M_x\text{Mo}_6\text{T}_8$ compounds ($x \approx 1$) is a well-known^{20,21} adaptation of cavity 1 to cation insertion (Figure 5b–f), which appears as (i) variations in the cation CN and (ii) almost linear correlations (for the rhombohedral phases) between the cation sizes, cations’ delocalization, and the M_i –Mo distances (Figure 7). As a result of lower delocalization and higher M_1 –Mo distances, the potential energy of the sites in cavity 1 decreases for larger cations. In contrast, the geometry of cavity 2 at this intercalation level remains almost unchangeable: the M_2 –Mo and M_3 –Mo distances for CPs with different cations are very close. The sizes of the interstitials in cavity 2 are similar to those of the host and suitable only for insertion of small cations. This

steric inconvenience or apparent suppression of the interstitials in cavity 2 can be estimated by a relative difference between the sites’ BVS values and the formal cation charge V : $(\text{BVS}-V)/V$ (Figure 8). As can be seen, the increase in the apparent suppression with cation size is more drastic for the central sites in cavity 2 than for the outer ones. A combination of the larger steric inconvenience and the shorter M_i –Mo distances for larger cations results in the higher potential energy for all the sites in cavity 2, but especially for the central ones.

It is clear that the diffusion activation energies depend not only on the atomic positions in the crystal structure, but also on the cation charge, as well as on the character of the M –Mo and M –T interactions. However, the BVS values and the M_i –Mo distances unambiguously testify: The larger are the inserted cations M , the higher is the difference between the potential energies of the sites in cavities 2 and 1, i.e., the larger are the activation energy of the progressive motion, E_d , whereas the bottleneck of the cation diffusion is

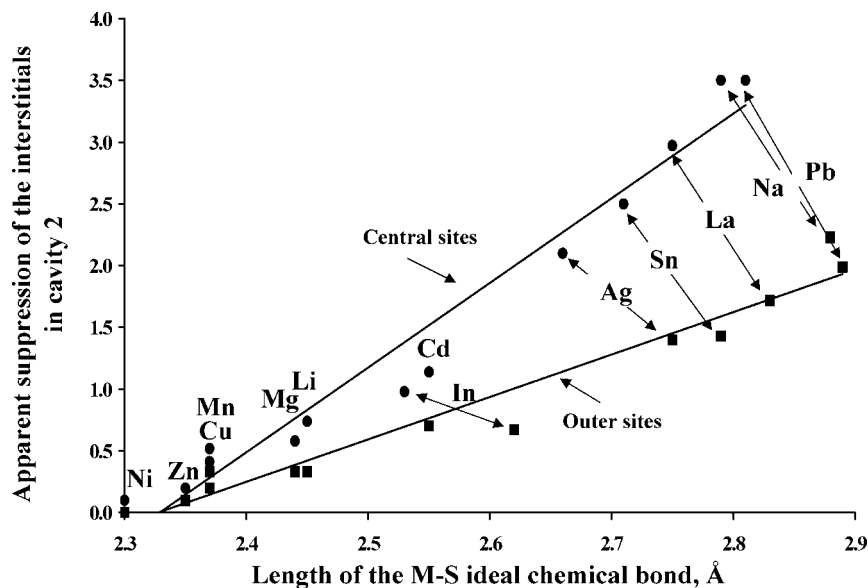


Figure 8. Correlations between the lengths of the ideal chemical bonds “cation–anion” and apparent suppression of the interstitials in cavity 2.

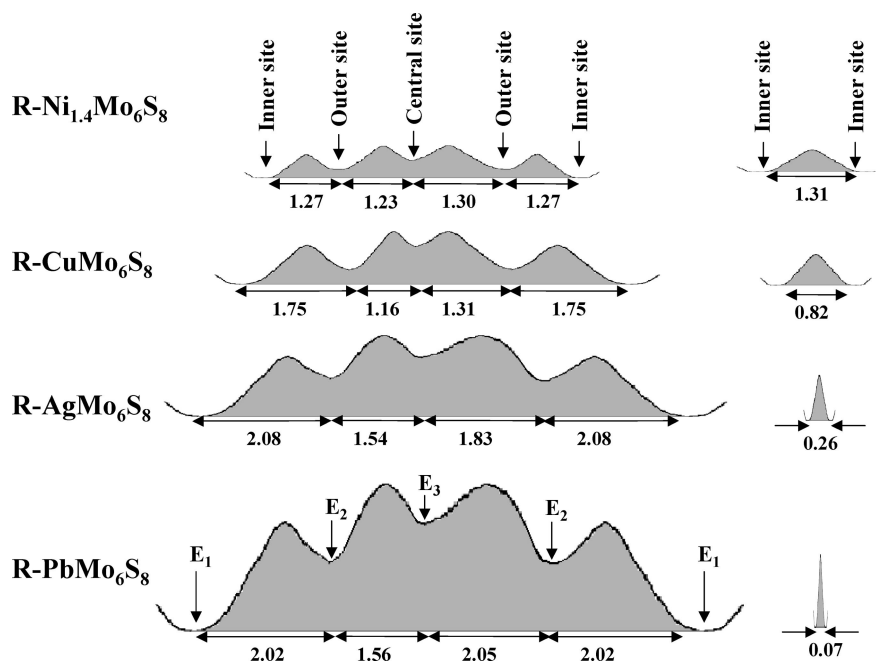


Figure 9. Schematic relative changes in the potential energy throughout the diffusion pathways for CPs with different mobility of inserted cations.

the central sites in cavity 2. The increase in E_d should be accompanied by a decrease in the activation energy of the circular motion, E_c , because of the lower diameter of the inner ring (i.e., because of a combination of the shorter hopping distances and the lower potential energy for the inner sites). As a result, the circular motion becomes more favorable than the progressive one. These changes of the potential energy throughout the diffusion pathways for the CPs with different cation mobility can be illustrated in schematic relative way (Figure 9). Thus, the cation size itself has no pronounced effect on the ionic mobility of the intercalated species in CPs, but in most of the cases it determines the cation position in the crystal structure, and consequently, the E_d/E_c ratio.

Repulsion between the Inserting Cations. The variation in the E_d/E_c ratio explains well the difference in the ionic

conductivity of large and small cations in CPs, but is still insufficient to clarify all the phenomena such as the insertion of large cations like Na^+ or K^+ at RT, the increase in the cation mobility for higher intercalation stages, and trapping or coupled diffusion with assistance of big cations. These phenomena can be understood only by taking into account the repulsion between the inserting cations as a driving force of the progressive diffusion (the latter can be roughly estimated by their metallic radius, i.e., the repulsion should decrease in the following sequence: $\text{K} > \text{Na} > \text{Pb} > \text{In} > \text{Mg} > \text{Sn} > \text{Cd} > \text{Li} > \text{Ag} > \text{Zn} > \text{Mn} > \text{Cu} > \text{Ni}$).

For small cations, such as Ni, Zn, and Li, their low repulsion is not so important, because the activation energies of the two competing diffusion pathways are low and very close: $E_d/E_c \approx 1$. As a result, these ions are highly mobile in the whole intercalation range ($0 < x < 2$). For larger

cations, like Cu^+ and Mn^{2+} , the circular motion in their sulfides, MMo_6S_8 , is energetically more attractive than the progressive one: $E_d > E_c$. This results in relatively slow cation diffusion at the first intercalation stages ($x < 1$). Only the cation repulsion upon insertion of the second or third cation (in the Cu^+ case) per formula unit leads to the fast ionic transport (a similar mechanism can be proposed for the Cd^{2+} mobility in the $\text{Cd-Mo}_6\text{Se}_8$ system).

An additional increase in the E_d/E_c ratio for the $\text{Mg-Mo}_6\text{S}_8$, $\text{Cd-Mo}_6\text{S}_8$, and $\text{Na-Mo}_6\text{T}_8$ systems results in the phenomenon of partial cation trapping. It can be suggested that such big monovalent ions like K^+ and Na^+ can progressively move in the CPs structure only because of their high cation-cation repulsion. This suggestion agrees well with overvoltage typical for the Na electrochemical insertion and trapping upon its extraction. For large divalent cations, such as Sn^{2+} and Pb^{2+} , $E_d \gg E_c$, thereby their progressive diffusion in the microcrystalline Mo_6T_8 is impossible. However, these cations can be inserted into the thin films. Moreover, trapped or "immobile" cations become mobile in the quaternary CPs upon coupled diffusion based on the presence of different cations in the same group of sites and their mutual repulsion. Thus, the CPs crystal structure is sufficiently flexible to provide progressive diffusion of large cations such as K^+ , Na^+ , Ag^+ , Sn^{2+} , and Pb^{2+} in case where the pushing forces of the inserted cations (related to their mutual repulsion) are high enough to overcome the E_d energetic barriers.

Typical examples of more detailed diffusion analysis can be found in the Supporting Information.

Conclusion

A general structural approach was used for the first time to explain the peculiarities of the cation transport in a variety of CPs at RT, such as: (i) immobility of large cations like Pb^{2+} , Sn^{2+} , Ag^+ in the ternary phases, MMo_6T_8 ; (ii) coupled $\text{M} + \text{M}'$ cation diffusion, which can include the mass-transport of the large cations, in the quaternary phases, $\text{M}_x\text{M}'_y\text{Mo}_6\text{T}_8$; (iii) existence of partial cation trapping phenomena in the $\text{Mg-Mo}_6\text{S}_8$, $\text{Cd-Mo}_6\text{S}_8$, and $\text{Na-Mo}_6\text{T}_8$ systems at RT; (iv) a combination of slow and fast diffusion kinetics at the first and last intercalation stages, respectively, for the $\text{Cu-Mo}_6\text{S}_8$, $\text{Mn-Mo}_6\text{S}_8$, and $\text{Cd-Mo}_6\text{Se}_8$ systems; and (v) a fast ionic transport for small cations like Ni^{2+} , Zn^{2+}

and Li^+ . This approach includes: (i) analysis of the polyhedral linkages in the diffusion channels of CPs, which can be substantially different in the various CPs; (ii) mapping of all the cation sites combined with their BVS values and the distances from the adjacent Mo atoms. Such a combination allows us to not only know the hopping lengths but also estimate the energetic parameters of the separate jumps (potential energies of the cations sites and activation barriers).

The analysis shows two competing pathways for most CPs: circular motion between the inner sites with activation energy E_c , and progressive diffusion with four separate jumps from one cavity 1 (or 2) to the adjacent one, with activation energy E_d . Thus, the cation mobility in CPs at RT has three key contributions: two activation energies, E_d and E_c (or their ratio E_d/E_c), as well as the distribution of the repulsive forces between the inserted cations. The energies, E_d and E_c , are affected, in turn, by the cation position, its size, cation-Mo interactions, and the anion nature, whereas the third parameter is related to the repulsion between the inserted cation, their sites' arrangement, and their number for the group of sites, i.e., it depends on the intercalation level and the direction of the electrochemical reaction (insertion or extraction).

Important practical conclusion can be obtained from this work: In spite of the apparent ionic immobility for some compositions, the Mo_6 clusters in CPs ensure a high diffusivity (at RT) of mono- and divalent cations with a wide spectrum of sizes. The reason for this unusual phenomenon is an efficient attainment of local electroneutrality by the Mo_6 clusters upon cation insertion. Hence, a future development of new cathode materials for rechargeable Mg batteries should be focused on cluster-containing intercalation compounds.

Acknowledgment. Partial support for this work was obtained from the Israel-U.S. binational foundation (BSF). The Institut Laue Langevin is warmly acknowledged for providing the neutron facilities.

Supporting Information Available: Additional data relating to the mobility of different cations in CPs; maps of the cation sites for a variety of CPs, possible insertion mechanism for large cations, and typical examples of the diffusion analysis for the CPs with different cation mobility (PDF). This material is available free of charge via the Internet at <http://pubs.acs.org>.

CM900033V